Supplementary Information

Title: Organo tin precursors for synthesis of zeolite Sn-Beta for alcohol ring opening of epoxides

Authors: Alexander P. Spanos,[a] Leah Ford, [a] Jiawei Guo,[b] Ryan Burrows, [a] Dr. Ambarish Kulkarni[b] and Dr. Nicholas A. Brunelli*[,a]

Author address: [a] William G. Lowrie Department of Chemical and Biomolecular Engineering, The Ohio State University, 151 West Woodruff Avenue, Columbus, OH 43210, U.S.A.

[b] Department of Chemical Engineering, University of California, Davis, California, 95616, U.S.A.

***Corresponding author**; Email: brunelli.2@osu.edu; Twitter**:** OSUChemEProfBru

S1. Experimental methods

S1.1. Hydrothermal synthesis of Sn-Beta and alkyl-Sn-Beta

The synthesis of zeolite Beta with alkyl tin precursors is achieved through a modified procedure reported previously.[1] Briefly, tetraethylammonium hydroxide (12.7 g of 35 wt% aqueous solution) is diluted with DI water (25 g). In a glovebox under nitrogen atmosphere, 0.27 mmol of an alkyl tin trichloride (either methyl-$SnCl_3$, n-butyl-$SnCl_3$, or phenyl-$SnCl_3$; exact masses listed in Table S1) is weighed in a vial and dissolved in 1 g of tetra ethyl ortho silicate (TEOS) and then removed from the glovebox. In a 100 mL round bottom flask, TEOS (10.44 g) is added and mixed with a stir bar, followed by the addition of the diluted TEAOH solution. After mixing for 15 minutes, the TEOS/alkyl-tin mixture (11.44 g of TEOS in total) is added to the flask and loosely covered with parafilm. After allowing the mixture to hydrolyze for 20 hours, the mixture is rotovapped at 40°C to below the target weight, followed by the addition of DI water (10 mL). This is repeated for a total of three cycles to remove ethanol, followed by the addition of water to reach the target weight. The synthesis gel is then split evenly into two Teflon autoclave liners and 0.50 mL of 51 wt% HF solution was added to each reactor, giving a gel composition of 1 SiO_2 / 0.005 Sn / 0.54 TEAOH / 0.54 HF / 7.5 H_2O. The resulting thick gel is manually stirred with a Teflon rod, and Si-Beta seeds (5% of the expected SiO_2 weight) are added and homogenized. The liner is sealed in stainless steel autoclaves and heated at 140°C for a certain period of time, around 25 days. The solids are recovered by filtration, extensively washed with water, dried at 100°C overnight, and finally calcined at 550°C for 10 h to remove the organic content located in the crystalline material.

Table S1. Mass of Sn precursor used in the synthesis of zeolite Beta.

Sn Precursor	Mass (g)
$SnCl_4$	0.072
Me-$SnCl_3$	0.066
Bu-$SnCl_3$	0.077
Ph-$SnCl_3$	0.083

S1.2. Material Characterization

S1.2.1. Standard methods

The materials are analyzed using a series of standard characterization techniques, including nitrogen physisorption, powder X-ray diffraction (PXRD), diffuse reflectance infrared Fourier transform spectroscopy (DRIFTS), thermogravimetric analysis-differential scanning calorimetry (TGA-DSC), and elemental analysis.

The crystallinity of the materials is analyzed using PXRD and nitrogen physisorption. Nitrogen physisorption is performed on a Micromeritics 3Flex surface characterization analyzer. The samples are first degassed on a Micromeritics SmartVacPrep sample preparation device at 140ºC under vacuum (10^{-3} mmHg) for 16 h followed by an additional in-situ degassing step on the 3Flex for 4 h at 140ºC under vacuum ($5x10^{-5}$ mmHg). The nitrogen sorption isotherms of degassed samples are recorded at liquid nitrogen temperatures (~77 K). The surface area and micropore volume of the materials are reported using BET and the t-plot method, respectively. The PXRD is collected using a Bruker powder X-ray diffractometer in flat plate reflection, Bragg Brentano optics mode using Cu $K_{\alpha1}$- $K_{\alpha2}$ radiation (λ = 1.540 and 1.544 Å) at 40 kV, 40 mA, and room temperature.

DRIFTS analysis is performed using a Nicolet iS50 spectrometer equipped with MCT-A liquid nitrogen cooled detector (32 scans at 2 cm^{-1} resolution). The DRIFTS set up includes a Praying Mantis (Harrick Scientific Products, Inc.) with a high temperature reaction chamber consisting of zinc selenide (ZnSe) windows. The material is initially degassed *in situ* at 500°C for 60 minutes under nitrogen flow. The material is then cooled to 25°C and pulsed with deuterated-acetonitrile using a VICI 6-port valve equipped with 100 µL sample loop. The probe molecule is allowed to desorb under nitrogen flow while increasing the temperature from 25°C to 125°C in steps, holding for 10 minutes at each temperature. The IR spectra are collected using the degassed material at corresponding temperature before dosing as the background. The DRUV-vis spectra are collected on Evolution 300 UV-Vis spectrometer with a resolution of 2 nm at a rate of 10 nm/s with pure silica analogues of materials as the background.

The actual weight percent of heteroatom (Sn) substituted in the silica framework in the materials is analyzed by Galbraith Laboratories using inductively coupled plasma-optical emission spectroscopy (ICP-OES).

S1.2.2. Trimethyl phosphine oxide (TMPO) Dosing and ^{31}P MAS NMR

Trimethyl phosphine oxide (TMPO) is used as a probe molecule to characterize active Sn sites in the Sn-Beta materials. Briefly, 100 mg of catalyst is dehydrated under vacuum at 140°C overnight. The catalyst is then cooled down to room temperature and a 0.05 wt% of TMPO in DCM is added to reach a desired ratio of 50 mol% of TMPO to total Sn in the catalyst, and it is allowed to mix overnight. The solvent is then removed by heating the sample back to 140°C overnight under vacuum. The samples are moved into a glovebox and packed into 7 mm ceramic rotors. The rotors are removed from the glovebox and run on a 600 MHz Bruker NMR for ^{31}P MAS NMR.

S1.2.3. Catalytic Testing

The catalytic testing set-up includes a two neck 10 mL round bottom (RB) flask equipped with a condenser, a magnetic stir bar, and a septum. The RB is filled with 2 mL of a solution containing 0.4 M epoxide and diethylene glycol dibutyl ether (DGDE) as an internal standard in neat alcohol. A sample (40 µL) is taken and diluted with acetone (~2 mL) to serve as the initial concentration data point. The required amount of catalyst is then added to the RB to achieve a 0.4 mol% concentration of Sn (calculated through ICP-OES elemental analysis) in the reaction system. After adding the catalyst, the reaction set-up is immersed in a silicone oil bath that is pre-heated to 60°C. At specific times, a reusable stainless-steel needle is used to draw a sample (40 µL), which is filtered using a small plug of silica and diluted with acetone. The samples are analyzed using gas chromatography (Agilent, 7820A with a SH-Rtx-5MS that has a length of 15 m, ID 0.25 and DF 0.25) equipped with flame ionization detector (GC-FID). The conversion is computed using the internal standard method using the equation:

$$Conversion(t) = 100 * \left(1 - \frac{Integrated\ Area\ of\ Epoxide_t / Integrated\ Area\ of\ Internal\ Standard_t}{Integrated\ Area\ of\ Epoxide_{t=0} / Integrated\ Area\ of\ Internal\ Standard_{t=0}}\right)$$

Where the integrated area of the epoxide and internal standard are from the GC-FID data.

S2. Results and discussion

S2.1.Material Characterization - XRD

The materials are tested for crystallinity using XRD, as shown in Figure S1 with an inset of the 2Θ in Figure S2.

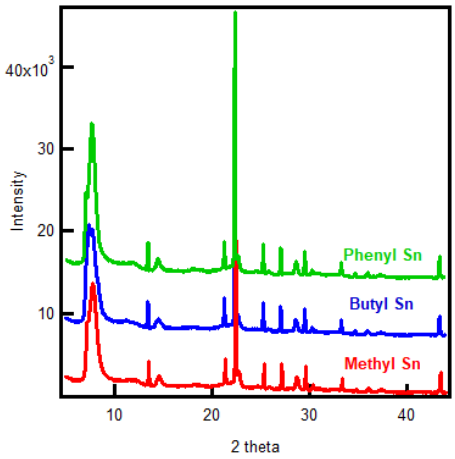

Figure S1. XRD patterns of Ph-Sn-Beta, Bu-Sn-Beta, and Me-Sn-Beta.

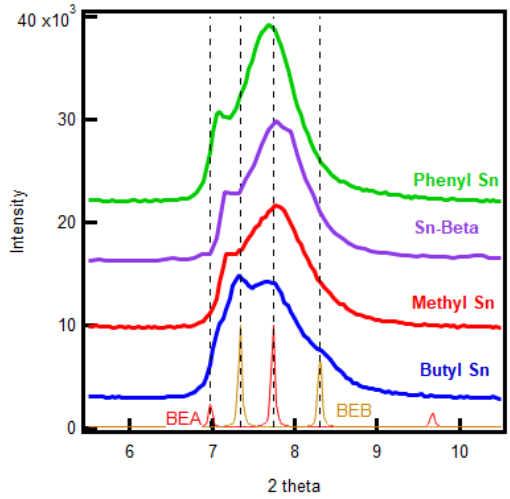

Figure S2. XRD patterns of Ph-Sn-Beta, Sn-Beta, Bu-Sn-Beta and Me-Sn-Beta with references for BEA and BEB frameworks from 2Θ of 5° to 10°.

S2.2.Material Characterization – Nitrogen physisorption

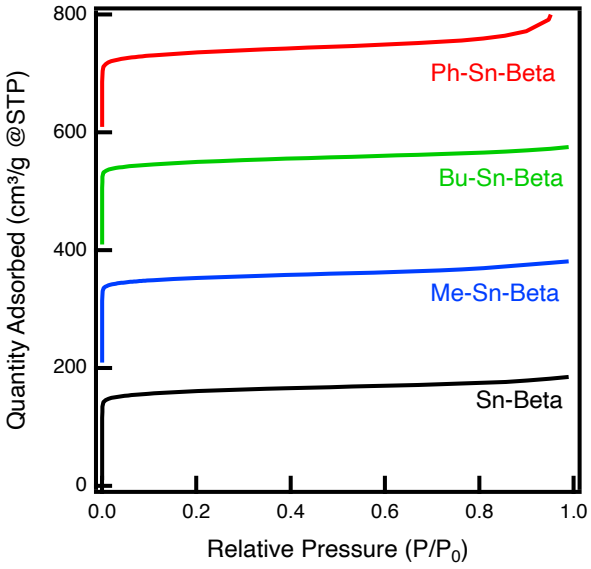

Figure S3. Comparison of nitrogen physisorption isotherms. The data are offset on the y-axis for clarity by increments of 200.

Table S2. Comparison of material properties.

Material	Micropore Volume (cm^3/g)[a]	Actual Si:Sn [b]	Open:Closed [c]
Me-Sn-Beta	0.20	242	0.27
Bu-Sn-Beta	0.19	282	0.39
Ph-Sn-Beta	0.20	245	0.32
Sn-Beta	0.21	218	0.22

[a] From nitrogen physisorption. [b] From ICP-OES. [c] From DRIFTS using deuterated acetonitrile. The value is the ratio of the integrated areas.

S2.3. Catalytic testing

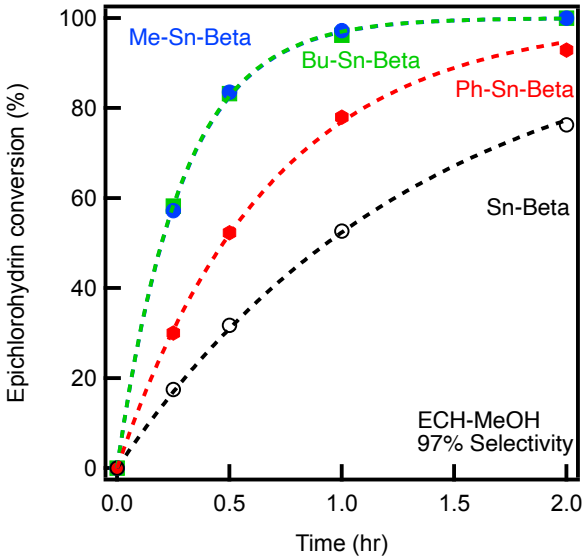

Figure S4. Catalytic testing of Ph-Sn-Beta, Bu-Sn-Beta and Me-Sn-Beta for epoxide ring opening of 0.4M epichlorohydrin in methanol at 60°C with a molar epoxide:Sn of 250:1.

Table S3. Material characteristics of Ph-Sn-Beta, Bu-Sn-Beta and Me-Sn-Beta.

Material	k (hr^{-1}) for ECH-MeOH	Selectivity for regiomer 4	k (hr^{-1}) for EH-MeOH	Selectivity for regiomer 4
Me-Sn-Beta	3.49±0.05	97	0.50±0.05	52
Bu-Sn-Beta	3.50±0.04	97	0.89±0.05	56
Ph-Sn-Beta	1.47±0.03	97	1.30±0.10	44

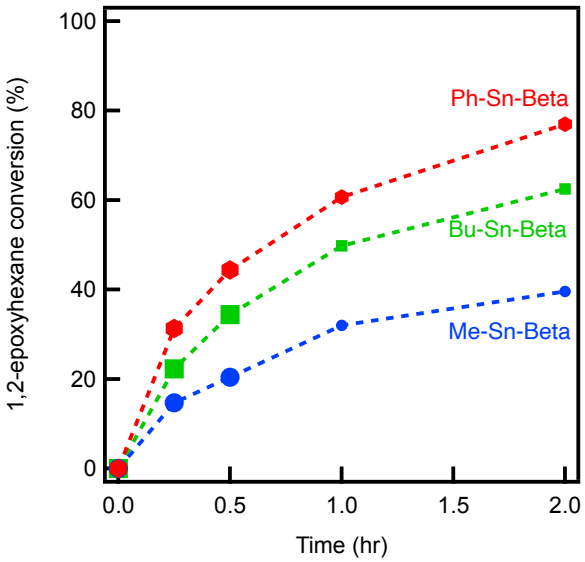

Figure S5. Catalytic testing of Ph-Sn-Beta, Bu-Sn-Beta and Me-Sn-Beta for epoxide ring opening of 0.4M 1,2-epoxyhexane (EH) in methanol (MeOH) at 60°C with a molar epoxide:Sn of 250:1. The dashed lines are used to connect the data.

S2.4.Material Characterization – DRIFTS

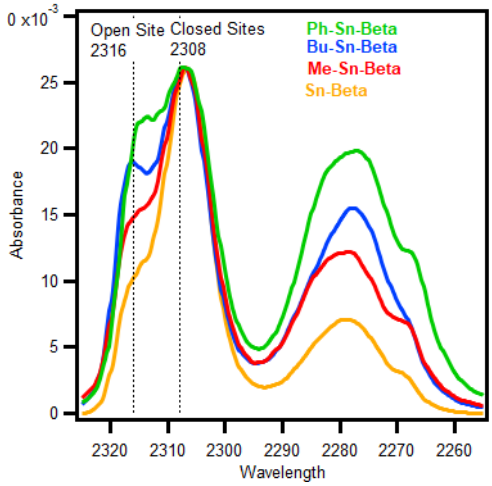

Figure S6. DRIFTS Spectra of d3-ACN saturated onto Ph-Sn-Beta, Bu-Sn-Beta, Me-Sn-Beta and conventional Sn-Beta normalized by the peak closed peak at 2308 cm^{-1}. Dashed lines indicate peak locations for open sites (2316 cm^{-1}) and closed sites (2308 cm^{-1}).

S2.5. Computational details & *DFT simulation of defect structure formation:*

The AIMD simulations were performed using the Vienna Ab-initio Simulation Package (VASP)[2–4] (version 5.4.4, ultrasoft pseudopotentials[5,6]), with a plane-wave cut-off of 300 eV, Perdew-Burke-Ernzerhof (RPBE) functional[7] and the default NELM of 60. Dispersion interactions were included using the Grimme D3 method with Becke-Jonson damping.[8,9] A 1e-6 eV energy cut-off was used as the convergence criteria for the electronic self-consistency cycle. A T5 cluster model was used with the alkyl groups attached to the T9 site in Sn-Beta. Cluster extracting and re-insertion are done through the MAZE package (https://github.com/kul-group/MAZE-sim/tree/master/maze).[10] The van der Waals parameters used to capture the interaction between alkyl groups and the framework Si are listed in the table below:

Lennard-Johns parameters	Sigma (Angstrom)	Epsilon (Kelvin)
CH3_sp3	108.0	3.76
Si_	22.0	2.30

To predict the local defect structure formed due to the alkyl-Sn site, we calculated the interaction energy of the alkyl group (modelled as a united atom) with each of the four neighboring Si atom. The AIMD trajectory of the alkyl groups, obtained using ab-initio molecular dynamics simulations of the 5-T cluster, is re-inserted in the periodic BEA framework to obtain the distances between the relevant atoms. Using the van der Waals radii as a proxy for steric effects (grey volumes), we observe considerable differences in the excluded volume for different alkyl groups. As united atom force fields are well-suited to describe the necessary framework- hydrocarbon interactions,[11] we calculate the pairwise interaction energy of the alkyl group with the individual "nearby" Si atoms (Fig. S7a) for each snapshot of the AIMD simulation described above (Fig. S7b). For Si atoms that are too close (i.e., distance < average Lennard-Jones distance (sigmaavg), the black line in Fig.

S7c and d) the interaction energy is repulsive (i.e., positive) and represents an energy penalty (Epenalty) that blocks the "nearby" Si atom. More importantly, the probability of defect formation (i.e., "Si atom being removed caused by the alkyl-Sn precursor") is directly related to Epenalty using Boltzmann statistics (Fig. 4e). Figure S7 illustrates the above workflow for methyl- and phenyl-Sn; the unfavorable atoms for methyl-Sn (i.e., Si1) and phenyl- Sn (i.e., Si1, Si2) precursors are quantitatively identified. Note that Si3 and Si4 (Epenalty ~ 0 eV) remain unaffected, showing that for the T9 site considered here, the phenyl-Sn precursor will result in a larger silanol defect than the methyl-Sn analogue.

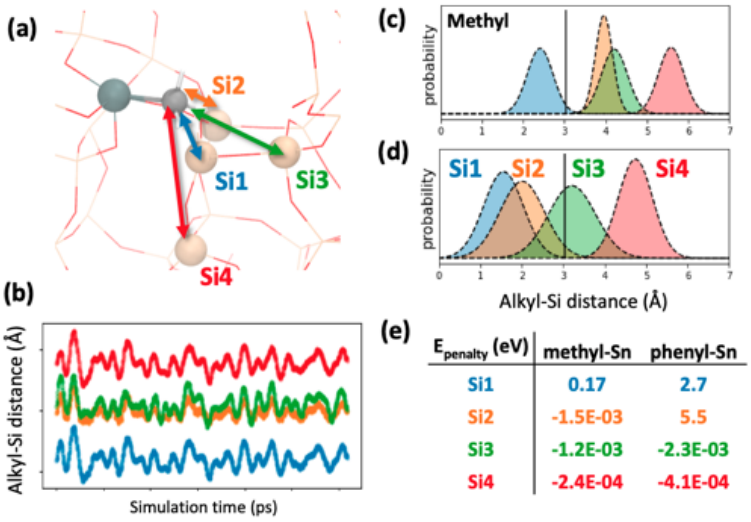

$E_{penalty}$ (eV)	methyl-Sn	phenyl-Sn
Si1	0.17	2.7
Si2	-1.5E-03	5.5
Si3	-1.2E-03	-2.3E-03
Si4	-2.4E-04	-4.1E-04

Figure S7. Overview of the combined AIMD and force field approach to calculate the energy penalty for the formation of defective silanol nests for several different alkyl-Sn precursors. (a) Representative image showing the individual C_{CH3-Si} distances for the T9 site in BEA. (b) Variation of the C_{CH3-Si}-Si distance over a 5 ps AIMD simulation. Histogram of the C_{CH3-Si}-Si distances for (c) methyl and (d) phenyl-Sn precursors. (e) Energy penalty values obtained using UFF model, suggesting the formation of 1Si defect (Si1 is sterically hindered) for methyl- and 2Si defect (Si1 and Si2 are both sterically hindered) phenyl-Sn.

S3. References

1 N. Deshpande, A. Parulkar, R. Joshi, B. Diep, A. R. Kulkarni and N. A. Brunelli, *J. Catal.*, 2019, **370**, 46–54.

2 G. Kresse and J. Furthmüller, *Computational Materials Science*, 1996, **6**, 15–50.

3 G. Kresse and J. Furthmüller, *Phys. Rev. B*, 1996, **54**, 11169–11186.

4 G. Kresse and J. Hafner, *Phys. Rev. B*, 1994, **49**, 14251–14269.

5 G. Kresse and D. Joubert, *Phys. Rev. B*, 1999, **59**, 1758–1775.

6 K. Lejaeghere, G. Bihlmayer, T. Björkman, P. Blaha, S. Blügel, V. Blum, D. Caliste, I. E. Castelli, S. J. Clark, A. Dal Corso, S. De Gironcoli, T. Deutsch, J. K. Dewhurst, I. Di Marco, C. Draxl, M. Dułak, O. Eriksson, J. A. Flores-Livas, K. F. Garrity, L. Genovese, P. Giannozzi, M. Giantomassi, S. Goedecker, X. Gonze, O. Grånäs, E. K. U. Gross, A. Gulans, F. Gygi, D. R. Hamann, P. J. Hasnip, N. A. W. Holzwarth, D. Iuşan, D. B. Jochym, F. Jollet, D. Jones, G. Kresse, K. Koepernik, E. Küçükbenli, Y. O. Kvashnin, I. L. M. Locht, S. Lubeck, M. Marsman, N. Marzari, U. Nitzsche, L. Nordström, T. Ozaki, L.

Paulatto, C. J. Pickard, W. Poelmans, M. I. J. Probert, K. Refson, M. Richter, G.-M. Rignanese, S. Saha, M. Scheffler, M. Schlipf, K. Schwarz, S. Sharma, F. Tavazza, P. Thunström, A. Tkatchenko, M. Torrent, D. Vanderbilt, M. J. Van Setten, V. Van Speybroeck, J. M. Wills, J. R. Yates, G.-X. Zhang and S. Cottenier, *Science*, 2016, **351**, aad3000.

7 J. P. Perdew, K. Burke and M. Ernzerhof, *Phys. Rev. Lett.*, 1996, **77**, 3865–3868.

8 S. Grimme, S. Ehrlich and L. Goerigk, *J Comput Chem*, 2011, **32**, 1456–1465.

9 S. Grimme, J. Antony, S. Ehrlich and H. Krieg, *The Journal of Chemical Physics*, 2010, **132**, 154104.

10 D. D. Antonio, J. Guo, S. J. Holton and A. R. Kulkarni, *SoftwareX*, 2021, **16**, 100797.

11 A. Abdelrasoul, H. Zhang, C.-H. Cheng and H. Doan, *Microporous and Mesoporous Materials*, 2017, **242**, 294–348.